RSC Advances

PAPER

View Article Online
View Journal | View Issue

Cite this: *RSC Adv.*, 2026, **16**, 29012

Magnorolins A–L: sesquiterpenoids with diverse skeletons from the fruits of *Magnolia grandiflora* and their cytotoxic and anti-inflammatory activities

Qiu-Ye Zhao,[ab] Shi-Huan Yin,[ab] Xin-Ying Wang,[ab] Lu Sai,[ab] Lin-Fen Ding*[b] and Xing-De Wu *[a]

Phytochemical investigation on the fruits of *Magnolia grandiflora* L. (Magnoliaceae) led to the isolation and characterization of sixteen sesquiterpenoids, including twelve previously undescribed sesquiterpenoids with diverse carbon skeletons, magnorolins A–L (**1–3**, **5–12**, and **15**), and four known analogues. Their structures were established by detailed spectroscopic methods, NMR, HR-ESI-MS, ECD calculations, and single-crystal X-ray diffraction analysis. Notably, compound **1** represents an unprecedented C17-germacrene-type sesquiterpenoid bearing a 1,7-dioxaspiro[4.4]nonane moiety; compounds **5** and **6** are rare C18-guaiane-type sesquiterpenoids; and compounds **8** and **9** are unusual guaiane-type sesquiterpenoids characterized by an oxygen bridge between C-6 and C-10. The isolated compounds were evaluated for biological activity *in vitro*, revealing that **3**, **4**, **13**, **14**, and **16** exhibited potent cytotoxic activities against five human cancer cell lines (K562, A549, HepG2, MDA-MB-231, and SW480) with IC_{50} values ranging from 6.07 to 31.15 μM. Furthermore, compounds **3**, **4**, **13**, and **16** showed strong inhibitory effects on lipopolysaccharide-induced nitric oxide release in RAW 264.7 macrophages, with IC_{50} values of 14.46 ± 0.12, 6.74 ± 0.05, 6.03 ± 0.09, and 12.20 ± 0.13 μM, respectively. This study enriches the structural diversity of sesquiterpenoids from *M. grandiflora* and provides valuable experimental basis for the further development and utilization of this plant in innovative drug discovery.

Received 1st April 2026
Accepted 19th May 2026

DOI: 10.1039/d6ra02737g

rsc.li/rsc-advances

1 Introduction

The genus *Magnolia*, belonging to the family Magnoliaceae, encompasses approximately 90 species globally. These species are distributed across temperate and tropical regions of southeastern Asia, including northeastern India, the Malay Archipelago, and Japan, as well as southeastern North America, Central America, and the Greater and Lesser Antilles.[1] In China, around 31 species are found, ranging from the southwest and southern areas of the Qinling Mountains to East and Northeast China.[1] *Magnolia* species are notable for their abundant natural resources, extensive medicinal history, and widespread clinical applications. For example, the flower buds of *Magnolia denudata*, known as "Xinyi" in traditional Chinese medicine, are commonly employed to treat conditions such as rhinitis, headaches, chills, and hypotension.[2,3] Contemporary phytochemical investigations have revealed that *Magnolia* species are rich in structurally diverse secondary metabolites, primarily including alkaloids, lignans, flavonoids, phenylethanoid glycosides, and terpenoids.[4–8] Within the terpenoid class, sesquiterpenoids represent the most abundant terpenoid constituents in this genus, with major skeleton types such as germacrane, eudesmane, and guaiane.[9–11] Notably, sesquiterpenoids like parthenolide, costunolide, reynosin, and santamarine are widely found in various *Magnolia* species.[12,13] Modern pharmacological studies have confirmed that sesquiterpenoids from *Magnolia* plants exhibit a range of significant biological activities, including anti-inflammatory, anticancer, antiprotozoal, and antioxidant effects.[10,14–17] These findings underscore their considerable potential for development and highlight their substantial scientific value in the field of innovative drug discovery and development.

Magnolia grandiflora L., a species belonging to the genus *Magnolia* (Magnoliaceae), is indigenous to southeastern North America and has been widely cultivated in urban regions south of the Yangtze River Basin in China.[18] Both the flowers and bark of this species possess medicinal properties, with documented pharmacological effects including antihypertensive activity, as well as the ability to dispel wind and alleviate cold symptoms.[19,20] Previous phytochemical studies on the twigs and leaves of *M. grandiflora* have revealed that this plant is a rich source of sesquiterpenoids, which demonstrate a broad spectrum of biological activities such as anti-inflammatory, anticancer, and nematicidal.[10,11,15,21,22] In our earlier phytochemical

[a]*Laboratory of Ethnic Medicine Resource Chemistry, Ministry of Education, Yunnan Minzu University, Kunming, 650504, China. E-mail: wuxingdeymu@163.com*
[b]*School of Pharmaceutical Sciences & Yunnan Key Laboratory of Pharmacology for Natural Products, Kunming Medical University, Kunming 650500, China. E-mail: dinglinfen@kmmu.edu.cn*

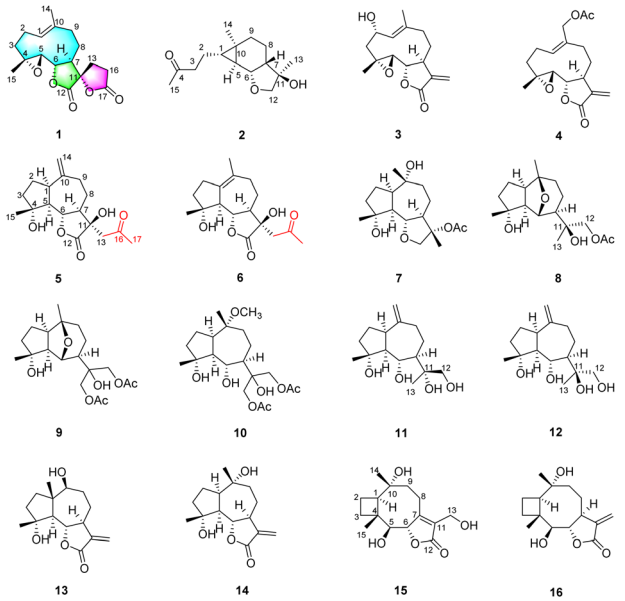

Fig. 1 Structures of compounds **1–16** isolated from *Magnolia grandiflora*.

investigations of the leaves of *M. grandiflora*, a series of sesquiterpenoids were isolated and identified; notably, 1,10-epoxyparthenolide and micheliolide exhibited significant cytotoxic effects mediated *via* the NF-κB signaling pathway.[14,23,24] However, there has been limited chemical investigation of the fruits of this species. To discover more structurally unique and biologically active sesquiterpenoids, we carried out an extensive phytochemical study on the fruits of *M. grandiflora*. In this study, sixteen sesquiterpenoids (Fig. 1) were isolated and characterized, including twelve previously undescribed compounds. The *in vitro* cytotoxicity of all isolated compounds was evaluated against five human cancer cell lines (K562, HepG2, A549, MDA-MB-231 and SW480) using the MTS assay. Additionally, the anti-inflammatory activities of compounds **1–14** and **16** were assessed by examining their inhibitory effects on lipopolysaccharide (LPS)-induced nitric oxide production (NO) in RAW 264.7 macrophage cells.

2 Results and discussion

2.1 Structure elucidation

Magnorolin A (**1**) was isolated as a colorless oil. Its molecular formula was established as $C_{17}H_{22}O_5$, corresponding to seven degrees of unsaturation, based on the deprotonated molecular ion observed at *m/z* 305.1391 $[M - H]^+$ (calcd for $C_{17}H_{21}O_5$, 305.1394) in the HR-ESI-MS analysis. The IR spectrum of **1** showed characteristic absorption bands at 1776, 1733, and 1709 cm^{-1}, indicative of ester carbonyl and olefinic functionalities, respectively. The ^1H NMR spectrum of **1** (Table 1) displayed signals assignable to a tertiary methyl at δ_H 1.31 (s, H_3-15), an olefinic methyl at δ_H 1.71 (s, H_3-14), an olefinic methine at δ_H 5.21 (d, $J = 10.1$ Hz, H-1), and two oxygenated methines at δ_H 2.78 (d, $J = 9.5$ Hz, H-5) and 3.89 (t, $J = 9.5$ Hz, H-6). Analysis of the ^{13}C NMR and DEPT spectra exhibited 17 carbon resonances (Table 2), comprising two methyl groups, six methylenes, four methines (one olefinic at δ_C 125.8 and two oxygenated at δ_C 66.2 and 80.3), and five nonprotonated carbons (one olefinic at δ_C 134.1, two ester carbonyls at δ_C 172.8 and 174.7, and two oxygenated at δ_C 62.0 and 85.0). The presence of one double bond and two ester carbonyl groups accounted for three of the seven degrees of unsaturation, suggesting that **1** is a homosesquiterpenoid featuring a tetracyclic ring system.

Table 1 ^1H (600 MHz) NMR data for compounds **1–3** and **5** in $CDCl_3$ (δ in ppm, J in Hz)

Position	1	2	3	5
1	5.21, d (10.1)	0.81, ddd, (8.5, 6.0, 4.9)	5.28, d, (11.3)	2.95, m
2a	2.40, m	1.70, m	4.67, td (11.3, 5.8)	1.77, m
2b	2.20, m	1.44, m		1.77, m
3a	2.16, m	2.53, t (7.4)	2.57, dd (11.3, 5.8)	1.88, m
3b	1.24, m		1.24, t (11.3)	1.80, m
5	2.78, d (9.5)	0.71, dd (8.0, 4.9)	2.85, d (8.9)	2.23, t (11.7)
6	3.89, t (9.5)	4.72, dd (8.0, 5.8)	3.82, t (8.9)	4.42, dd (11.7, 9.3)
7	2.66, t (9.5)	1.50, m	2.80, m	1.86, m
8a	1.90, dd (14.7, 6.9)	1.40, m	2.19, m	2.67, dt (12.0, 3.5)
8b	1.61, m	0.76, dd (13.8, 4.2)	1.71, m	1.78, m
9a	2.37, m	1.83, m	2.40, dd (12.8, 6.0)	1.78, m
9b	2.10, t (12.5)	1.38, m	2.22, t (12.8)	1.70, m
12a		3.60, d (9.3)		
12b		3.58, d (9.3)		
13a	2.35, m	1.21, s	6.34, d (3.4)	2.77, d (16.8)
13b	2.18, m		5.63, d (3.4)	2.63, d (16.8)
14a	1.71, s	1.09, s	1.77, s	4.97, s
14b				4.93, s
15	1.31, s	2.14, s	1.29, s	1.32, s
16a	2.90, dt (17.8, 10.4)			
16b	2. 61, ddd (17.8, 9.7, 2.4)			
17				2.32, s

Table 2 ^{13}C (150 MHz) NMR data for compounds **1–3**, and **5–7** in $CDCl_3$. (δ in ppm)

Position	1	2	3	5	6	7
1	125.8	21.2	129.2	44.3	132.1	49.7
2	24.1	23.6	66.6	26.5	30.2	25.6
3	36.8	43.8	45.3	40.3	38.7	39.6
4	62.0	209.7	60.8	80.2	80.7	80.1
5	66.2	28.1	66.5	55.9	58.4	55.6
6	80.3	76.0	82.2	84.1	83.5	81.3
7	49.5	48.6	47.7	53.0	55.7	55.5
8	25.2	20.1	30.4	26.1	21.9	22.3
9	40.8	30.3	41.4	38.8	35.1	45.1
10	134.1	21.4	136.5	148.1	131.5	75.1
11	85.0	81.1	139.0	75.9	76.3	86.7
12	172.8	78.0	169.3	175.7	175.7	77.2
13	25.4	20.6	121.6	44.4	43.6	18.3
14	16.9	20.8	17.9	112.3	23.9	23.6
15	17.2	30.4	18.5	24.4	23.2	23.4
16	27.3			210.3	210.9	
17	174.7			32.3	32.4	
11-$OCOCH_3$						170.6
11-$OCOCH_3$						21.8

The gross structure of **1** was initially elucidated through an extensive analysis of its 2D NMR data (Fig. 2). The ^1H–^1H COSY spectrum revealed the presence of three spin systems: –CH–CH_2–CH_2– (for C-1/C-2/C-3), –CH_2–CH_2– (for C-13/C-16) and –CH–CH–CH–CH_2–CH_2– (for C-5/C-6/C-7/C-8/C-9). HMBC correlations of H_2-2 [δ_H 2.40 (m, H-2a); 2.20 (m, H-2b)] and H_2-9 [δ_H 2.37 (m, H-9a); 2.10 (t, J = 12.5 Hz, H-9b)] and H_3-14 with C-1 (δ_C 125.8) and C-10 (δ_C 134.1), as well as of H_3-15 with C-3 (δ_C 36.8), C-4 (δ_C 62.0), and C-5 (δ_C 66.2), suggested the presence of a 10-membered carbocyclic ring featuring a trisubstituted double bond between C-1 and C-10, along with two methyl groups at C-4 and C-10. The chemical shifts observed for C-4 (δ_C 62.0) and C-5 (δ_C 66.2) suggested the incorporation of a trisubstituted 4,5-epoxide moiety within **1**, which was further supported by key HMBC correlations of H-5 to C-3, C-4, C-6 (δ_C 80.3), and C-7 (δ_C 49.5). Additional HMBC cross-peaks from H-6 to C-11 (δ_C 85.0) and C-12 (δ_C 172.8) indicated the presence of a 12,6-lactone ring fused to the 10-membered carbocyclic ring *via* C-6 and C-7. Furthermore, a 17,11-lactone ring was identified as being connected to the 12,6-lactone ring through the spiro carbon at C-11, as evidenced by HMBC correlations from H_2-13 [δ_H 2.35 (m, H-13a) and 2.18 (m, H-13b)] to C-7, C-11 and C-12, as well as from H-6 to C-11 and C-12, in conjunction with the chemical shift of C-11 at δ_C 85.0. Collectively, these data established **1** as a novel homogermacrane sesquiterpenoid featuring a 1,7-dioxaspiro [4.4]nonane structural motif.

The relative configuration of **1** was determined through analysis of the ROESY spectrum. Key ROESY correlations (Fig. 3) between H-5 and H-7, as well as between H-6 and H_3-15, indicated that H-5 and H-7 are α-oriented, while H-6 and H_3-15 are β-oriented. Additionally, diagnostic ROESY correlations between H-6 and H-13a established the *S** configuration at the C-11 spiro carbon atom. The *E*-geometry of the $\Delta^{1,10}$ double bond was further confirmed by cross-peaks observed H-1/H-9b and H-2a/H_3-14 in the ROESY spectrum. Ultimately, the absolute configuration of **1** was assigned as 4*R*, 5*S*, 6*S*, 7*R*, 11*S* based on the comparison of experimental and calculated ECD spectra (Fig. 5).

A plausible biosynthetic pathway for **1**, originating from parthenolide, was proposed as illustrated in Scheme 1. It is hypothesized that parthenolide undergoes enzymatic epoxidation at the $\Delta^{11,13}$ position, resulting in the formation of intermediate. (i) This epoxide subsequently undergoes a nucleophilic ring-opening reaction through conjugate addition of acetyl-SCoA, wherein the enolate derived from acetyl-SCoA attacks the electrophilic epoxide, yielding the thioester intermediate. (ii) Hydrolysis of the thioester moiety under acidic conditions then produces the carboxylic acid intermediate. (iii) Finally, intermediate (iii) undergoes intramolecular

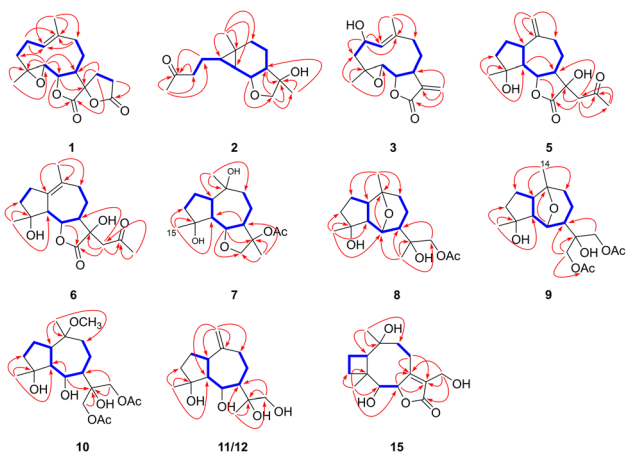

Fig. 2 Key ^1H–^1H COSY and HMBC correlations of **1–3**, **5–12**, and **15**.

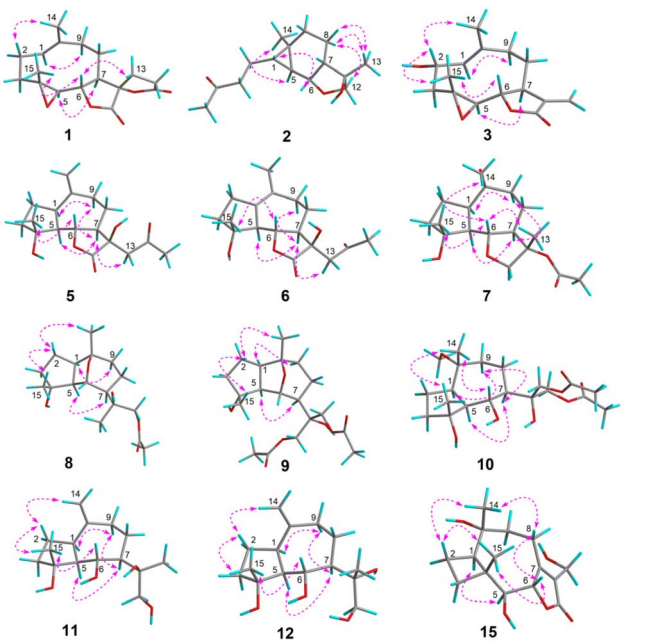

Fig. 3 Key ROESY correlations of **1–3**, **5–13**, and **15**.

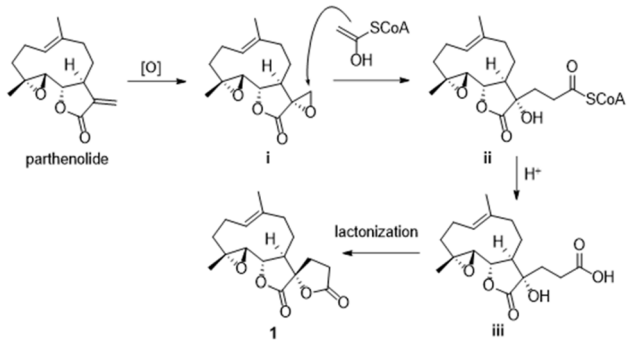

Scheme 1 A plausible biosynthetic pathway for **1**.

lactonization, facilitated by the nucleophilic attack of the carboxylic acid on the adjacent hydroxy group, thereby forming the five-membered lactone ring and affording the final product **1**.

Magnorolin B (**2**) was isolated as a colorless oil, and its molecular formula was established as $C_{15}H_{24}O_3$ based on HR-ESI-MS data (*m/z* 275.1616 $[M + Na]^+$, calcd for $C_{15}H_{24}O_3Na$, 275.1618). The ^1H NMR data of **2** (Table 1) showed the existence of three methyl groups [1.21 (s, H_3-13), 1.09 (s, H_3-14), and δ_H 2.14 (s, H_3-15)]. Corresponding to the molecular formula, all 15 carbon signals (Table 2) were clearly resolved in the ^{13}C NMR spectrum and were classified by HSQC experiments as three methyls, five methylenes (including one oxygenated carbon), four methines (including one oxygenated carbon), and three quaternary carbons (including one keto carbonyl and one oxygenated carbon). The ^1H–^1H COSY correlations (Fig. 2) of H_2-3/H_2-2/H-1/H-5/H-6/H-7/H_2-8/H_2-9 indicated the presence of only one partial structure characterized by the sequence –CH_2-CH_2CHCHCHCHCH$_2$CH_2–. The HMBC spectrum exhibited key cross-peaks from H_3-14 to C-1 (δ_C 21.2), C-5 (δ_C 28.1), C-9 (δ_C 30.3), and C-10 (δ_C 21.4); from H_3-15 to C-3 (δ_C 43.8) and C-4 (δ_C 209.7); and from both H_2-12 (δ_H 3.60, d, J = 9.3 Hz; 3.58, d, J = 9.3 Hz) and H_3-13 to C-7 (δ_C 48.6) and C-11 (δ_C 81.1). Comprehensive analysis of these spectroscopic data suggested that **2** is a carabrane-type sesquiterpenoid.[25] The chemical shift of C-4 at δ_C 209.7 revealed the presence of a keto carbonyl group in **2**, which was further corroborated by key HMBC correlations of H_2-2 [δ_H 1.70 (m, H-2a) and 1.44 (m, H-2b)], H_2-3 [δ_H 2.53 (t, J = 7.4 Hz)], and H_3-15 to C-4. The formation of a five-membered oxygen-containing heterocyclic ring between C-6 (δ_C 76.0) and C-12 (δ_C 78.0) was substantiated by HMBC correlation from H-6 [δ_H 4.72 (dd, J = 8.0, 5.8 Hz)] to C-12. Additionally, the presence of an 11-OH group was proved by HMBC correlations from H-7 (δ_H 1.50, m), H_2-12, and H_3-13 to C-11. The relative configuration of **2** was determined through analysis of the ROESY spectrum (Fig. 3). The correlations of H_3-14/H-5, H-6/H-1, H-8a/H_3-13, H-8b/H_3-13, and H-12a/H-8b suggested that H-5, H_3-13, and H_3-14 are oriented in the α-position, whereas H-1, H-6, and H-7 occupy the β-orientation. The absolute configuration of **2** was determined as 1*S*, 5*S*, 6*R*, 7*S*, 10*R*, 11*R* by comparing the experimental and calculated ECD spectra (Fig. 5).

Magnorolin C (**3**) was obtained as colorless crystals. Its molecular formula was determined to be $C_{15}H_{20}O_4$ by HR-ESI-MS, which showed an ion peak at *m/z* 287.1255 $[M + Na]^+$ (calcd for $C_{15}H_{20}O_4Na$, 287.1254). Examination of the ^1H and ^{13}C NMR data (Tables 1 and 2) suggested that **3** is a germacra-12,6-olide sesquiterpenoid, structurally similar to parthenolide.[26] The primary distinction is the presence of a hydroxy group at C-2 (δ_C 66.6) in **3**. This deduction was confirmed by HMBC correlations (Fig. 2) from H-2 [δ_H 4.67 (td, J = 11.3, 5.8 Hz)] to C-1 (δ_C 129.2), C-3 (δ_C 45.3), and C-10 (δ_C 136.5), along with the notable downfield shift observed at C-2 ($\Delta\delta_C$ 66.6). In the ROESY spectrum (Fig. 3), cross-peaks observed between H-5 and H-7 indicated that these protons are on the same face and assigned to be α-oriented. Conversely, ROESY correlations of H-2/H_3-15 and H-6/H_3-15 suggested that H-2, H-6, and H_3-15 are co-facial and assigned as β-oriented. The *E*-configuration of the $\Delta^{1,10}$ double bond was determined by ROESY correlations of H-1/H-9b and H-2/H_3-14. To further confirm the planar structure and determine the absolute configuration, single-crystal X-ray diffraction analysis was performed (Fig. 4). As a result, the absolute configuration of **3** was determined to be 2*S*, 4*R*, 5*S*, 6*S*, 7*S*, with Flack parameter of −0.04(7).

Magnorolin D (**5**), a corlorless oil, has a molecular formula $C_{17}H_{24}O_5$ based on the HR-ESI-MS ion at *m/z* 331.1515 $[M + Na]^+$ (calcd for $C_{17}H_{24}O_5Na$, 331.1516), corresponding to six degrees of unsaturation. Its IR spectrum revealed characteristic absorption bands corresponding to hydroxy (3419 cm^{-1}), ketone carbonyl (1774 cm^{-1}), ester carbonyl (1710 cm^{-1}), and double bond (1638 cm^{-1}) functional groups. Analysis of the ^1H and ^{13}C NMR spectra, along with the HSQC spectrum, revealed resonances (Tables 1 and 2) corresponding to two methyls [δ_H 1.32 (s, H_3-15) and 2.32 (s, H_3-17); δ_C 24.4 (C-15) and 32.3 (C-17)], six methylenes including one was olefinic [δ_H 4.97 (s, H-14a) and 4.93 (s, H-14b); δ_C 112.3 (C-14)], four methines with one oxygenated [δ_H 4.42 (dd, J = 11.7, 9.3 Hz, H-6); δ_C 84.1 (C-6)], and five nonprotonated carbons, including one olefinic carbon [δ_C 148.1 (C-10)], two oxygenated carbons [δ_C 80.2 (C-4) and 75.9 (C-11)], a ketone carbonyl [δ_C 210.3 (C-16)], and an ester carbonyl [δ_C 175.7 (C-12)].

The ^1H–^1H COSY (Fig. 2) correlations of H_2-3/H_2-2/H-1/H-5/H-6/H-7/H_2-8/H_2-9 indicated the presence of a single partial structure [–CH_2–CH_2CH-CHCHCHCH$_2$CH_2–]. Furthermore, HMBC cross-peaks from H-6 to C-12 supported the structural assignment. Collectively, these spectroscopic data supported

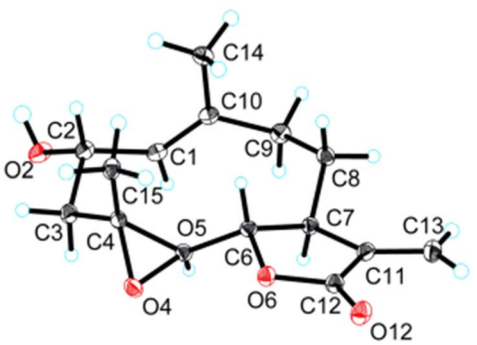

Fig. 4 X-ray structure of **3**.

the identification of **5** as a C18-homoguaia-12,6-olide sesquiterpenoid. The terminal $\Delta^{10,14}$ double bond was confirmed by HMBC correlations from H_2-14 to C-1 (δ_C 44.3), C-9 (δ_C 38.8), and C-10. Additionally, HMBC correlations of H_2-13 [δ_H 2.77 (d, J = 16.8 Hz, H-13a) and 2.63 (d, J = 16.8 Hz, H-13b)] to C-7 (δ_C 53.0), C-11, C-12, C-16, and C-17, along with correlations from H_3-17 to C-13 (δ_C 44.4) and C-16, implied that the presence of a 2-oxopropyl group at C-11. ROESY cross-peaks (Fig. 3) between H-1/H-9a, H-5/H-7, H-7/H-9a, H-7/H_2-13, and H_3-15/H-6 indicated the α-orientations of H-1, H-5, and H-7, whereas the β-orientations of H-6, H_3-15, and 11-OH. The absolute configuration of **5** was determined to be 1*R*, 4*R*, 5*S*, 6*S*, 7*R*, 11*R* by comparison of the experimental and calculated ECD spectra (Fig. 5).

Magnorolin E (**6**), a colorless oil, was found to have the same molecular formula, $C_{17}H_{24}O_5$, as **5**, based on HR-ESI-MS and ^{13}C NMR analyses. The ^1H and ^{13}C NMR spectroscopic data of **6** (Tables 2 and 3) were similar to those of **5**, except that the C-10/C-14 double bond in **5** was shifted to C-1/C-10 in **6**. This finding was clarified by key HMBC correlations (Fig. 2) from H_3-14 (δ_H 1.68, s) to C-1 (δ_C 132.1), C-9 (δ_C 35.1), and C-10 (δ_C 131.5). The relative configurations at C-4, C-5, C-6, C-7, and C-11 of **6** were assigned as identical to those in **5**, based on ROESY data analysis (Fig. 3). Furthermore, the calculated ECD spectrum of **6** showed good agreement with the experimental spectrum (Fig. 5), enabling the definitive assignment of its absolute configuration as 4*R*, 5*S*, 6*S*, 7*R*, 11*R*.

Magnorolin F (**7**) was obtained as a colorless oil. HR-ESI-MS analysis established its molecular formula as $C_{17}H_{28}O_5$, evidenced by a sodium adduct at m/z 335.1829 $[M + Na]^+$ (calcd for $C_{17}H_{28}O_5Na$, 335.1829), corresponding to four degrees of unsaturation. The ^1H and ^{13}C NMR spectroscopic data (Tables 2 and 3) of **7** displayed signals corresponding to one acetyl group [δ_H 2.01 (s); δ_C 21.8, 170.6], three methyl groups [δ_H 1.42 (s, H_3-13), 1.17 (s, H_3-14), and 1.25 (s, H_3-15); δ_C 18.3 (C-13), 23.6 (C-14), and 23.4 (C-15)], and five methylene groups including one oxygenated methylene [δ_H 3.99 (d, J = 9.7 Hz, H-12a) and 3.89 (d, J = 9.7 Hz, H-12b); δ_C 77.2 (C-12)]. Additionally, four methine carbons were observed, one of which was oxygenated [δ_H 3.67 (t, J = 10.8 Hz, H-6); δ_C 81.3 (C-6)], alongside four quaternary carbons, three of which were oxygenated sp3 carbons at δ_C 80.1 (C-4), 75.1 (C-10), and 86.7 (C-11). The HMBC spectrum (Fig. 2) revealed correlations from H_3-15 to C-3 (δ_C 39.6), C-4 (δ_C 80.1), and C-5 (δ_C 55.6); from H_3-14 to C-1 (δ_C 49.7), C-9 (δ_C 45.1), and C-10; from H_3-13 to C-7 (δ_C 55.5), C-11, and C-12. The ^1H–^1H COSY spectrum demonstrated correlations among H-1, H_2-2, and H_2-3, as well as between H-5, H_2-6, H-7, H_2-8, and H_2-9. Furthermore, the chemical shifts of C-6 (δ_C 81.3) and C-12 (δ_C 77.2), along with the HMBC correlations from H-6 to C-11 and C-12, demonstrated the presence of a five-membered oxygen-containing heterocyclic ring between C-6 and C-12, consistent with the structural motif observed in **2**. Consequently, compound **7** was characterized as a guaiene sesquiterpenoid featuring an 8-oxabicyclo[5.3.0]decane unit.

A comparison of the ^1H and ^{13}C NMR spectra of **7** with those of magnograndiolide[27] indicated that both compounds share an identical 5/7 bicyclic ring system featuring two hydroxy groups located at C-4 and C-10. This structural assignment was corroborated by HMBC correlations observed from H_3-14 to C-1, C-9, and C-10, as well as H_3-15 to C-3, C-4 and C-5. Additionally,

Table 3 ^1H (600 MHz) NMR data for compounds **6–9** in $CDCl_3$ (δ in ppm, J in Hz)

Position	6	7	8	9
1		2.47, ddd (13.3, 10.5, 8.5)	2.45, td (8.5, 3.6)	2.86, d (8.3)
2a	2.38, dd (16.1, 8.0)	1.90, m	1.79, m	1.79, m
2b	2.18, m	1.55, m	1.64, m	1,64, m
3a	1.80, m	1.78, m	1.58, m	1.86, m
3b	1.76, m	1.74, m	1.53, m	1.53, m
5	2.58, d (10.3)	2.20, dd (13.3, 10.8)	2.78, d (8.5)	2.47, td (8.5, 3.5)
6	4.32, t (10.3)	3.67, t (10.8)	4.26, s	4.21, s
7	1.72, m	1.95, m	1.70, m	1.86, m
8a	1.64, m	1.99, m	1.73, m	1.53, m
8b	1.56, m	1.27, m	1.58, m	1.58, m
9a	2.23, m	1.92, m	1.51, m	1.53, m
9b	2.10, t (13.7)	1.57, m	1.48, m	1.53, m
12a		3.99, d (9.7)	3.98, d (11.1)	4.09, s
12b		3.89, d (9.7)	3.89, d (11.1)	3.99, s
13a	2.76, d (16.7)	1.42, s	1.27, s	4.16, d (11.4)
13b	2.63, d (16.7)			4.11, s
14a	1.68, s	1.17, s	1.18, s	1.36, s
14b				
15	1.33, s	1.25, s	1.36, s	1.19, s
16a				
16b				
17	2.34, s			
11-$OCOCH_3$		2.01, s		
12-$OCOCH_3$			2.08, s	2.08, s
13-$OCOCH_3$				2.08, s

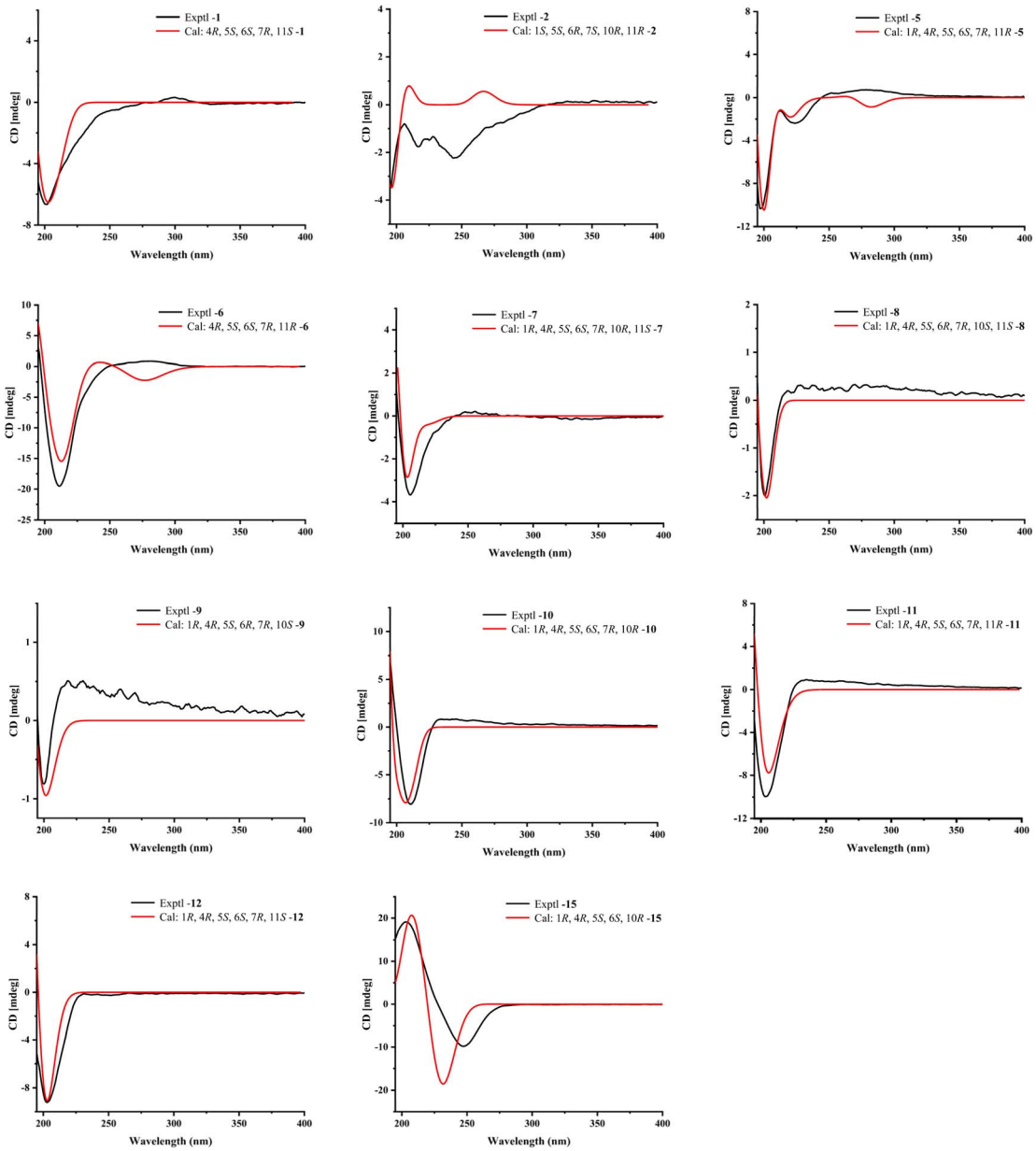

Fig. 5 Experimental and calculated ECD spectra of **1**, **2**, **5**–**12**, and **15**.

the chemical shift of C-11 (δ_C 86.7) exhibited a downfield shift of 5.6 ppm relative to the corresponding signal in **2** (δ_C 81.1), implying the presence of an acetoxy substituent at C-11. The relative configuration of **7** was determined through ROESY (Fig. 3) correlations of H-1/H-9b, H-5/H-7, H-7/H-9b, H-6/H_3-13, H-6/H_3-14, and H-6/H_3-15 confirmed the α-orientations of H-1, H-5, and H-7, as well as the β-orientations of H-6, H_3-13, H_3-14, and H_3-15. The absolute configuration of **7** was confirmed as 1*R*, 4*R*, 5*S*, 6*S*, 7*R*, 10*R*, 11*S* through ECD calculations (Fig. 5).

Magnorolin G (**8**) was isolated as a colorless oil with the molecular formula $C_{17}H_{28}O_5$, as determined by HR-ESI-MS showing a peak at *m*/*z* 335.1829 $[M + Na]^+$ (calcd for $C_{17}H_{28}O_5Na$, 335.1829), suggesting four degrees of unsaturation. The ^{1}H NMR spectrum (Tables 3 and 4) showed signals for three tertiary methyls [δ_H 1.27 (s, H_3-13), 1.18 (s, H_3-14), and 1.36 (s, H_3-15)], an acetyl methyl [δ_H 2.08 (s)], an oxygenated methylene [δ_H 3.98 (d, J = 11.1 Hz, H-12a) and 3.89 (d, J = 11.1 Hz, H-12b)], and an oxygenated methine [δ_H 4.26 (s, H-6)]. The ^{13}C NMR spectrum (Table 4) exhibited 17 carbon resonances, which were assigned as four methyls (δ_C 25.0, 23.7, 22.7, and 21.1), five sp3 methylenes (δ_C 70.0, 42.0, 38.1, 26.1, and 18.2), four methines (δ_C 77.4, 58.0, 50.1, and 45.1) including one oxygenated methine, three sp3 quaternary carbons (δ_C 81.9, 81.8, and 72.2), and an ester carboxyl carbon (δ_C 171.4). A thorough analysis of these ^{1}H and ^{13}C NMR data suggested that **8** is a guaiane-type sesquiterpenoid containing one acetyl group. The acetoxy group was inferred to be located at C-12 by HMBC correlations (Fig. 2) of H_2-12 with the ester carbonyl group.

Table 4 ^{13}C (150 MHz) NMR data for compounds **8**–**12**, and **15** (δ in ppm)

Position	**8** [a]	**9** [a]	**10** [a]	**11** [a]	**12** [a]	**15** [b]
1	50.1	58.1	44.8	41.7	41.6	49.9
2	26.1	26.1	25.2	25.3	25.1	18.8
3	42.0	17.9	41.3	40.8	41.0	33.2
4	81.9	81.9	82.5	81.2	81.6	45.2
5	58.0	50.1	56.5	57.0	56.8	86.5
6	77.4	77.0	75.6	76.4	75.6	86.3
7	45.1	41.7	49.9	53.8	49.0	169.5
8	18.2	38.1	24.8	29.4	29.1	22.2
9	38.1	41.9	39.8	39.5	38.8	42.0
10	81.8	81.9	77.7	149.4	149.5	73.9
11	72.2	73.0	76.5	77.3	77.3	129.4
12	70.0	65.2	68.0	67.4	69.8	174.9
13	23.7	65.0	66.1	26.0	20.3	54.1
14	22.7	24.9	20.9	109.8	109.4	24.0
15	25.0	22.7	22.2	22.9	22.6	16.1
12-OCOCH$_3$	171.4	171.2	171.3			
12-OCOCH$_3$	21.1	21.0	21.1			
13-OCOCH$_3$		171.1	171.2			
13-OCOCH$_3$		21.0	21.1			
10-OCH$_3$			48.2			

[a] Recorded in $CDCl_3$. [b] Recorded in CD_3OD.

HMBC cross-peak from H-6 to C-10 (δ_C 81.8) indicated that C-6 (δ_C 77.4) and C-10 are connected *via* an oxygen bridge. The ROESY spectrum of **8** showed correlations (Fig. 3) of H-5/H-7, H-1/H-9a, H$_3$-15/H-2b, and H-2b/H$_3$-14, indicating the α-orientations of H-1, H-5, and H-7, as well as the β-orientations of H$_3$-15 and the oxygen bridge between C-6 and C-10. However, the stereochemistry at C-11 could not be established from the ROESY data. Therefore, quantum chemical NMR calculations were performed to determine the relative configuration at C-11. Two possible epimers, **8**-(11*R**) and **8**-(11*S**), were studied using Gauge-Independent Atomic Orbital (GIAO) NMR calculations at the mPW1PW91/6-311+G(d, p) level, including solvent effects modeled by the Polarizable Continuum Model (PCM). The calculated shielding tensors for both stereoisomers were statistically analyzed using DP4+ probability analysis. The results conclusively identified the **8**-(11*S**) epimer as the correct stereoisomer, with a DP4+ probability of 100%, thus confirming the stereochemistry at C-11 (Fig. S122). Finally, the experimental ECD spectrum of **8** matched very well with the calculated ECD spectrum for the (1*R*, 4*R*, 5*S*, 6*R*, 7*R*, 10*S*, 11*S*)-**8** stereoisomer (Fig. 5), allowing the assignment of the absolute configuration of **8** as 1*R*, 4*R*, 5*S*, 6*R*, 7*R*, 10*S*, 11*S*.

The molecular formula of magnorolin H (**9**) was determined to be $C_{19}H_{30}O_7$ based on sodiated molecular ion peak $[M + Na]^+$ at *m/z* 393.1885 (calcd 393.1884) observed in the HR-ESI-MS spectrum, which is 58 mass units greater than that of **8**. A comparison of the ^{13}C NMR data (Table 3) of **9** with those of **8** indicated that both share the same skeleton structure, except for the presence of an additional acetoxy group at C-13 in **9**. This assignment was further supported by HMBC correlations from H$_2$-13 [δ_H 4.16 (d, J = 11.4 Hz, H-13a) and 4.11 (s, H-13b)] to the ester carbonyl carbon at δ_C 171.1. Detailed analysis of the ROESY data (Fig. 3) indicated that the relative configurations of H-1, H-5, H-6, H-7, H$_3$-14, and H$_3$-15 in **9** were identical to those in **8**. The absolute configuration of **9** was determined through a comparative analysis of its experimental ECD spectrum with the corresponding calculated ECD curve. The experimental ECD data demonstrated a high degree of concordance with the theoretical spectrum, thereby unequivocally confirming the absolute configuration of **9** as 1*R*, 4*R*, 5*S*, 6*R*, 7*R*, 10*S* (Fig. 5).

Magnorolin I (**10**), a colorless oil, has a molecular formula of $C_{20}H_{34}O_8$, as determined by positive HR-ESI-MS *m/z* 425.2149 $[M + Na]^+$ (calcd for $C_{20}H_{34}O_8Na$, 425.2146), corresponding to four degrees of unsaturation. The ^{1}H and ^{13}C NMR spectral data (Tables 4 and 5) of **10** showed signals for one methoxy group, two acetyl groups, two singlet methyl groups, a hydroxy substituted methine, and three oxygenated tertiary carbons. A careful comparison of the ^{13}C NMR data of **10** (Table 4) with those of **9** indicated that those two compounds share the same carbon framework. The major differences included the disappear of the C-6 and C-10 oxygen bridge in **10**, and the presence of an additional hydroxy and a methoxy group in **10**. The methoxy group was inferred to be located at C-10 by HMBC correlation (Fig. 2) of 10-OCH$_3$ (δ_H 3.12, s) with C-10. The presence of the additional hydroxy group at C-6 was confirmed by HMBC correlations of H-6 [δ_H 4.15 (t, J = 10.7 Hz)] to C-5 (δ_C 56.5) and C-6 (δ_C 75.6), as well as the ^{1}H–^{1}H COSY correlations of H-5/H-6/H-7. In the ROESY spectrum (Fig. 3), the correlations of H-1/H-9b, H-5/H-7, H-7/H-9b, H-6/H$_3$-14, and H$_3$-15/H$_3$-14, establishing the α-orientations of H-1, H-5, and H-7, as well as the β-orientations of H-6, H$_3$-14, and H$_3$-15. The absolute configuration of 1*R*, 4*R*, 5*S*, 6*S*, 7*R*, 10*R* was assigned based on the agreement between the experimental and calculated ECD spectra of **10** (Fig. 5).

The molecular formula of magnorolins J (**11**) and K (**12**) was determined to be $C_{15}H_{26}O_4$ based on their HR-ESI-MS and ^{13}C NMR data. Their IR spectra showed distinctive hydroxy absorption bands at 3398 cm^{-1} for **11** and 3382 cm^{-1} for **12**, along with olefinic group absorptions at 1708 cm^{-1} for **11** and 1704 cm^{-1} for **12**) groups. The ^{1}H and ^{13}C NMR spectra (Tables 4 and 5) displayed 15 carbon signals, which included two methyl groups, six methylenes (including one oxygenated and one olefinic carbon), four methines (including one oxygenated carbon), one olefinic quaternary carbon, and two oxygenated tertiary carbons. The 1D NMR spectroscopic data of **11** were closely related to those of **10**, with notable differences including the absence of methoxy and acetyl groups, and the presence of a terminal double bond and a hydroxy group in **11**. In the HMBC spectrum (Fig. 2), correlations from H$_2$-14 [δ_H 4.90 (s, H-14a) and 4.83 (s, H-14b)] correlated to C-10 (δ_C 149.4), demonstrated the presence of a terminal $\Delta^{10,14}$ double bond. The acetoxy group at C-12 in **10** was replaced by a hydroxy group in **11**, as evidenced by HMBC correlations of H$_2$-12 [δ_H 3.81 (d, J = 10.8 Hz, H-13a) and 3.48 (d, J = 10.8 Hz, H-13b)] with C-11 (δ_C 77.3). The relative configuration of **11** was elucidated through ROESY correlations (Fig. 3), where interactions between H-1/H-9b, H-5/H-7, H-7/H-9b, H-2b/H-14a, H-2b/H$_3$-15, and H-6/H$_3$-15 indicated that H-1, H-5, and H-7 share the same face and were assigned as α-oriented, while H-6 and H$_3$-15 were assigned to be

Table 5 ^{1}H (600 MHz) NMR data for compounds **10**–**12** and **15** (δ in ppm, J in Hz)

Position	**10** [a]	**11** [a]	**12** [a]	**15** [b]
1	2.61, dd (13.0, 9.5)	2.91, m	2.91, m	2.12, dd (11.0, 8.1)
2a	1.82, m	1.80, m	1.79, m	1.98, m
2b	1.52, m	1.76, m	1.75, m	1.81 m
3a	1.88, m	1.82, m	1.77, m	1.78, m
3b	1.70, m	1.78, m	1.77, m	1.56, m
5	2.25, dd (13.0, 10.7)	2.20, t (10.9)	2.18, t (10.7)	3.21, d (9.0)
6	4.15, t (10.7)	3.92, dd (10.9, 8.5)	3.94, t (10.7)	4.88, d (9.0)
7	1.95, t (10.7)	1.88, m	1.99, m	
8a	1.72, m	1.92, m	1.84, m	3.01, dd (17.1, 10.3)
8b	1.17, m	1.36, m	1.23, m	2.47, dd (17.1, 10.3)
9a	1.91, m	2.46, m	2.47, m	2.01, dd (12.0, 10.3)
9b	1.38, td (13.2, 2.8)	1.94, m	1.93, m	1.72, dd (12.0, 10.3)
12a	4.28, d (11.1)	3.81, d (10.8)	3.58, d (11.1)	
12b	4.16, d (11.1)	3.48, d (10.8)	3.41, d (11.1)	
13a	4.42, d (11.0)	1.21, s	1.22, s	4.31, d (12.7)
13b	4.30, d (11.0)			4.26, d (12.7)
14a	1.08, s	4.90, s	4.88, s	1.30, s
14b		4.83, s	4.81, s	
15	1.34, s	1.28, s	1.31, s	1.32, s
12-OCOCH3	2.12, s			
13-OCOCH3	2,10, s			
10-OCH_3	3.12, s			

[a] Recorded in $CDCl_3$. [b] Recorded in CD_3OD.

β-oriented. However, the stereochemistry at C-11 could not be determined by the ROESY spectrum. Therefore, the relative configuration at C-11 was assigned as *R** based on DP4+ probability analysis, which involved comparing the experimental and calculated ^{13}C NMR chemical shifts (Fig. S125). The absolute configuration of **11** was established as 1*R*, 4*R*, 5*S*, 6*S*, 7*R*, 11*R* by comparing its experimental ECD spectrum with the calculated spectrum (Fig. 5).

Analysis of the 2D NMR data, including the ^{1}H–^{1}H COSY and HMBC spectra (Fig. 2), confirmed that **12** shares the same planar structure as **11**. A comparison of their ^{13}C NMR chemical shifts revealed that the primary differences occur at C-7 (δ_C 53.8 for **11**, δ_C 49.0 for **12**) and C-12 (δ_C 67.4 for **11**, δ_C 69.8 for **12**), indicating that these two compounds are a pair of 11-epimers. ROESY data analysis (Fig. 3) demonstrated that both compounds possess the same relative configurations at C-1, C-5, C-6, and C-7. Subsequently, ^{1}H and ^{13}C NMR calculations were conducted for **12**-11*S** and **12**-11*R**, and DP4+ probability analysis suggested that **12**-11*S** represents the correct configuration (Fig. S128). Finally, the absolute co-nfiguration of **12** was established as 1*R*, 4*R*, 5*S*, 6*S*, 7*R*, 11*S* based on ECD data (Fig. 5).

Magnorolin L (**15**) was obtained as a colorless oil and determined to have the molecular formula $C_{15}H_{22}O_5$, corresponding to five indices of hydrogen deficiency. This was established based on the (−)-HR-ESI-MS data, which showed a sodium adduct ion peak at m/z 281.1396 ($[M - H]^-$, calcd 281.1394). Detailed analysis of the ^{1}H and ^{13}C NMR spectra (Tables 4 and 5), coupled with the HSQC data, indicated the presence of two tertiary methyls [δ_H 1.30 (s, H_3-14) and 1.32 (s, H_3-15); δ_C 24.0 (C-14) and 16.1 (C-15)], five methylenes including one oxygenated carbon [δ_H 4.31 (d, J = 12.7 Hz, H-13a) and 4.26 (d, J = 12.7 Hz, H-13b); δ_C 54.1 (C-13)], three methines with two oxygenated carbon [δ_H 3.21 (d, J = 9.0 Hz, H-5) and 4.88 (d, J = 9.0 Hz, H-6); δ_C 86.5 (C-5) and 86.3 (C-6)], and five quaternary carbons, including a carbonyl at δ_C 174.9 (C-12), an oxygenated carbon at δ_C 73.9 (C-10), and two olefinic carbons at δ_C 169.5 (C-7) and 129.4 (C-11). These functionalities accounted for two of the five degrees of unsaturation, indicating the presence of a tricyclic ring system in **15**. Comparative analysis of the NMR data revealed that **15** possesses a structure closely resembling that of michampanolide (**16**), a michampane sesquiterpenoid isolated from the root bark of *M. champaca*.[28] The primary differences include the substitution of the terminal $\Delta^{11,13}$ double bond in **16** with a tetrasubstituted $\Delta^{7,11}$ double bond in **15**, as well as the presence of an additional hydroxy group at C-13 in **15**. HMBC correlations (Fig. 2) from H-6, H_2-8 [δ_H 3.01 (dd, J = 17.1, 10.3 Hz, H-8a); 2.47 (dd, J = 17.1, 10.3 Hz, H-8b)] and H_2-13 to C-7 and C-11 verified the existence of the double bond between C-7 and C-11. The presence of the 13-OH group was confirmed by HMBC correlations of H_2-13 to C-7, C-11, and C-12, as well as the chemical shift of C-13 at δ_C 54.1. ROESY (Fig. 3) correlations involving H-1/H-5, H-2a/H_3-14, H-2a/H_3-15, H-6/H_3-15, H-6/H-8b, and H-8b/H_3-14 established that H-1 and H-5 are α-oriented, whereas H-6, H_3-14, and H_3-15 are β-oriented. The experimental ECD of **15** aligned with computational ECD calculations, thereby confirming its absolute configuration as 1*R*, 4*R*, 5*S*, 6*S*, 10*R* (Fig. 5).

Based on NMR data analysis and comparison to the reported references, four known sesquiterpenoids were identified as liriochinolide F (**4**),[29] lyciumate (**13**),[30] magnograndiolide (**14**),[27] and michampanolide (**16**).[28]

2.2 Biological activity

All isolated compounds were evaluated for their cytotoxic effects against human cancer cell lines, including K562 (chronic myelogenous leukemia), A549 (lung adenocarcinoma), HepG2 (hepatocellular carcinoma), MDA-MB-231 (breast adenocarcinoma), and SW480 (colorectal adenocarcinoma), using the MTS assay, with doxorubicin (DOX) and taxol serving as positive controls. At a concentration of 40 μM, compounds **3**, **4**, **13**, **14**, and **16** demonstrated cytotoxic activity, achieving inhibition rates exceeding 50% across various cancer cell lines, ranging from 54.40 ± 0.91% to 100.67 ± 0.37% (Fig. 6). The remaining compounds did not exhibit significant activity, with inhibition rates below 50% in all tested cell lines. Subsequently, the IC_{50} values for the five active compounds (**3**, **4**, **13**, **14**, **16**) were determined. Compound **13** exhibited the most potent and broad-spectrum cytotoxicity (Table 6), with IC_{50} values of 6.07 ± 1.42, 14.24 ± 0.41, 15.23 ± 0.15, 21.47 ± 0.17, and 16.94 ± 0.51 μM against K562, A549, HepG2, MDA-MB-231, and SW480 cell, respectively. Notably, it showed the highest activity against K562 cells, highlighting significant potential for its further development as a promising anticancer lead compound. Compound **14** showed moderate cytotoxicity against all tested cell lines, with IC_{50} values ranging from 15.28 ± 0.24, to 28.46 ± 0.62 μM. Compound **4** exhibited selective activity, with IC_{50} values of 15.60 ± 0.38, 27.44 ± 1.13, 24.09 ± 0.67, and 16.12 ± 0.95 μM against K562, A549, MDA-MB-231, and SW480 cells, respectively. Compound **3** was active against K562 and SW480 cells (IC_{50} = 16.55 ± 0.31 and 23.58 ± 0.93 μM, respectively) but showed no activity (IC_{50} > 40 μM) against A549, HepG2, and MDA-MB-231 cells. Meanwhile, compound **16** exhibited moderate activity against K562 and MDA-MB-231 cells (IC_{50} = 24.35 ± 0.96 and 31.15 ± 1.33 μM, respectively) and was inactive against A549, HepG2, and SW480 cells.

Additionally, compounds **1–14**, and **16** were assessed for their ability to inhibit NO production in LPS-induced RAW 264.7 cells, with NG-monomethyl-L-arginine, monoacetate salt (L-NMMA) used as a positive control. At a concentration of 50 μM, compounds **3**, **4**, **14**, and **16** significantly inhibited NO production without causing cytotoxicity, achieving inhibition rates above 50%. Subsequently, the IC_{50} values of these compounds were determined. The results indicated that compounds **3**, **4**, **13**, and **16** demonstrated strong inhibitory effects, with IC_{50} values of 14.46 ± 0.12, 6.74 ± 0.05, 6.03 ± 0.09, and 12.20 ± 0.13 μM, respectively (Table 7).

Among the sixteen sesquiterpenoids, compounds **3**, **4**, **13**, **14**, and **16**, which all contain an 11,13-unsaturated γ-lactone ring, showed significant cytotoxic effects and NO inhibitory activity. The analysis suggests that the 11,13-unsaturated γ-lactone is the primary active functional group responsible these effects. Nevertheless, these initial findings need to be confirmed through more comprehensive and systematic experimental studies to validate the proposed structure–activity relationship.

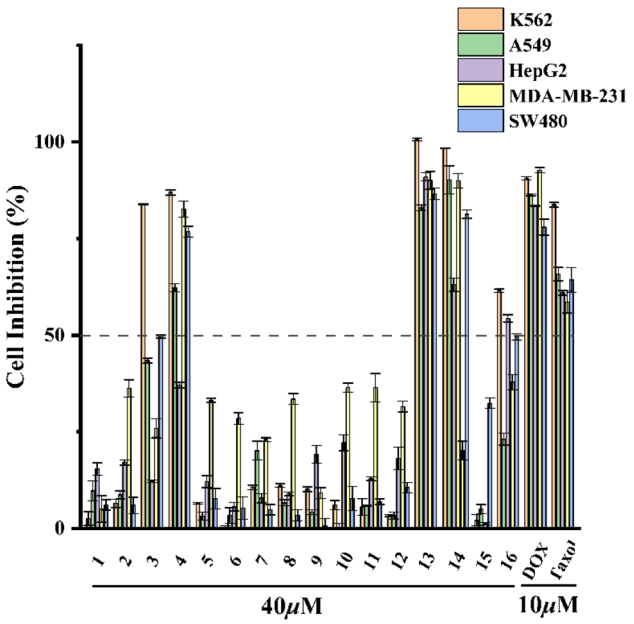

Fig. 6 Cell Inhibition (%) of **1–16** against five human cancer cell lines.

Table 7 Nitric oxide inhibitory activity of compounds **3**, **4**, **13** and **16**

Compound	IC_{50} (μM)
3	14.46 ± 0.12
4	6.74 ± 0.05
13	6.03 ± 0.09
16	12.20 ± 0.13
L-NMMA[a]	44.60 ± 1.00

[a] Positive control.

Table 6 Cytotoxic activity of compounds **1–16** against five cancer cells

Compound[a]	K562	A549	HepG2	MDA-MB-231	SW480
3	16.55 ± 0.31	>40	>40	>40	23.58 ± 0.93
4	15.60 ± 0.38	27.44 ± 1.13	>40	24.09 ± 0.67	16.12 ± 0.95
13	6.07 ± 1.42	14.24 ± 0.41	15.23 ± 0.15	21.47 ± 0.17	16.94 ± 0.51
14	15.28 ± 0.24	18.31 ± 0.45	28.46 ± 0.62	21.42 ± 0.26	18.11 ± 1.21
16	24.35 ± 0.96	>40	>40	31.15 ± 1.33	>40
DOX[b]	0.363 ± 0.048	0.576 ± 0.051	0.288 ± 0.006	0.234 ± 0.016	0.186 ± 0.033
Taxol[b]	<0.016	<0.016	<0.016	<0.016	<0.016

[a] IC_{50} of compounds **1**, **2**, **5–12**, **15** were over 40 μM for all tested cell lines. [b] Positive control.

3 Conclusions

In conclusion, sixteen structurally diverse sesquiterpenoids, including twelve previously unidentified sesquiterpenoids were isolated from the fruits of *M. grandiflora.* Compound **1** represents an unprecedented C17-germacrane-type sesquiterpenoid featuring a 1,7-dioxaspiro[4.4]nonane moiety. Compounds **5** and **6** are uncommon C18-guaiane-type sesquiterpenoids, further broadening the structural diversity of guaiane-type sesquiterpenoids. Compounds **2** and **7** are unique carabrane and guaiane sesquiterpenoids, respectively, each featuring an 8-oxabicyclo [5.3.0]decane unit that distinguishes them from other known analogs. Moreover, compounds **8** and **9** are unusual guaiane-type sesquiterpenoids featuring an oxygen bridge between C-6 and C-10, adding to the structural variety of guaiane-derived compounds. Among the isolated compounds, compound **13** showed the highest activity against K562 cell line with an IC_{50} value of 6.07 ± 1.42 μM. Overall, this study provides a systematic and comprehensive characterization of the sesquiterpenoid composition in the fruits of *M. grandiflora*, and enriches the structural diversity of sesquiterpenoids from the genus *Magnolia*. The biological activity findings provide a valuable experimental basis for further exploration and utilization of *M. grandiflora* as a promising source for discovering new anticancer lead compounds, paving the way for future detailed pharmacological studies and structural modifications of these sesquiterpenoids.

4 Experimental

4.1 General experimental procedures

1D and 2D NMR spectra were recorded on a Bruker Avance III 600 spectrometer. High-resolution electrospray ionization mass spectrometry (HR-ESI-MS) data were acquired on a Shimadzu UPLC IT-TOF mass spectrometer. Optical rotations were measured using a Jasco P-1020 polarimeter. Ultraviolet (UV) spectra were recorded using a Shimadzu UV2700 spectrophotometer. Infrared (IR) spectra were recorded on a Bruker Tensor-27 spectrometer employing potassium bromide (KBr) pellets. Medium-pressure liquid chromatography (MPLC) was performed on a Lisui EZ Purify III System (Shanghai LiSui Chemical Engineering Co., Ltd, Shanghai, China). Column chromatography (CC) was carried out over MCI gel (CHP 20P, 75−150 μm; Mitsubishi Chemical Corporation, Tokyo, Japan) and silica gel (100−200 mesh and 200−300 mesh; Qingdao Marine Chemical Co., Qingdao, China). Thin layer chromatography (TLC) analyses were carried out on precoated silica gel GF_{254} plates (SiO_2; Qingdao Haiyang Chemical Co., Qingdao, China). Semipreparative high performance liquid chromatography (semi-prep HPLC) was conducted on an Agilent 1260 system equipped with an Agilent Zorbax SB-C_{18} column (9.4 × 250 mm, 5 μm). Solvents including petroleum ether, chloroform, ethyl acetate, and methanol were sourced from Shanghai Titan Technology Co., Ltd (Shanghai, P. R. China).

4.2 Plant material

The fruits of *Magnolia grandiflora* L. were collected in July 2022 at Yunnan Minzu University, Yunnan province, China. The plant material was taxonomically identified by Professor Jing Zhou from Kunming Medical University. A voucher specimen (No. 202010m) has been deposited at the Key Laboratory of Ethnic Medicine Resource Chemistry, Ministry of Education, Yunnan Minzu University, China.

4.3 Extraction and isolation

Dried fruits of *M. grandiflora* (45 kg) were extracted with methanol (MeOH) three times at room temperature, each extraction lasting 48 h. The resulting concentrated extract (4.8 kg) was suspended in water and partitioned with ethyl acetate (EtOAc) to remove lipophilic components. The EtOAc-solube fraction (1.6 kg) was subjected to silica gel column chromatography (CC) eluted with petroleum ether (PE)-EtOAc (1 : 0–1 : 1, v/v), which yielded six fractions (Fr.1-Fr.6).

Fraction 4 (215.8 g) was further chromatographed over MCI gel using MeOH–H_2O (50 : 50–100 : 0, v/v) to afford eight subfractions (Fr.4.1-Fr.4.8). Compound **15** (6.8 mg) was obtained from Fr.4.2 (1.2914 g) *via* repeated silica gel CC. Fr.4.4 (571.8 mg) was first separated by silica gel CC and then purified by semi-preparative HPLC (MeOH–H_2O, 45 : 55, v/v), yielding compounds **5** (8.0 mg, t_R = 33.9 min) and **6** (6.1 mg, t_R = 44.9 min). Fr.5 (154.5 g) was fractionated by MCI gel with MeOH–H_2O (40 : 60–90 : 10, v/v) to give nine subfractions (Fr.5.1-Fr.5.9). Fr.5.3 (4.1170 g) was chromatographed on silica gel CC with CH_2Cl_2-acetone (200 : 1–1 : 1, v/v), affording seven subfractions (Fr.5.3.1-Fr.5.3.7). Compounds **13** (11.5 mg, t_R = 30.5 min) and **16** (2.0 mg, t_R = 18.7 min) were isolated from Fr.5.3.3 (200.0 mg) by repeated silica gel CC followed by semi-preparative HPLC (MeCN–H_2O, 25 : 75, v/v). Compound **14** (7.3 mg, t_R = 32.9 min) was purified from Fr.5.3.4 (241.7 mg) using semi-preparative HPLC (MeOH–H_2O, 73 : 27, v/v). Fr.5.4 (5.903 g) was subjected to silica gel CC eluted with CH_2Cl_2-acetone (1 : 0–1 : 1, v/v), yielding six subfractions (Fr.5.4.1-Fr.5.4.6). Fr.5.4.2 (592.5 mg) was further separated by silica gel CC with PE-acetone (8 : 1–1 : 1, v/v) to afford four subfractions (Fr.5.4.2.1-Fr.5.4.2.4). Compound **3** (12.8 mg, t_R = 59.4 min) was obtained from Fr.5.4.2.4 (221.3 mg) by semi-preparative HPLC (MeCN–H_2O, 14 : 86, v/v). Fr.5.4.5 (2.0115 g) was chromatographed on silica gel CC with PE-acetone (8 : 1–1 : 1, v/v) to afford five subfractions (Fr.5.4.5.1-Fr.5.4.5.5), and compound **8** (18.7 mg, t_R = 29.7 min) was purified from Fr.5.4.5.2 (72.7 mg) *via* semi-preparative HPLC (MeCN–H_2O, 20 : 80, v/v). Fr.5.5 (3.5532 g) was separated by silica gel CC and then purified by semi-preparative HPLC (MeCN–H_2O, 20 : 80, v/v), to obtained compound **9** (14.3 mg, t_R = 40.7 min). Fr.5.6 (4.2669 g) was separated by silica gel CC using CH_2Cl_2-acetone (200 : 1–1 : 1, v/v), yielding five subfractions (Fr.5.6.1-Fr.5.6.5). Compound **2** (13.0 mg, t_R = 15.6 min) was isolated from Fr.5.6.1 (220.1 mg) by repeated silica gel CC and subsequent semi-preparative HPLC (MeCN–H_2O, 35 : 65, v/v). Fr.5.6.3 (855.6 mg) was separated by repeated silica gel CC followed by semi-preparative HPLC (MeCN–H_2O, 28 : 72, v/v) to afford compound **10** (6.8 mg, t_R = 29.7 min). Compounds **11** (2.5 mg, t_R = 17.5 min) and **12** (4.0 mg, t_R = 19.8 min) were obtained from Fr.5.6.4 (1.0188 g) *via* semi-preparative HPLC (MeCN–H_2O, 28 : 72, v/v). Fr.5.7 (4.7932 g) was subjected to

silica gel CC and further purified by semi-preparative HPLC ($MeCNH_2O$, 38 : 72, v/v), affording compound **1** (3.2 mg, t_R = 45.5 min), while compound **4** (6.3 mg, t_R = 34.3 min) was isolated from Fr.5.8 (10.3812 g) using semi-preparative HPLC (MeCN–H_2O, 30 : 70, v/v). Fr.6 (159.0 g was fractionated by MCI gel with MeOH–H_2O (40 : 60–90 : 10, v/v) to give ten subfractions (Fr.6.1-Fr.6.10). Fr.6.5 (9.0548 g) was further separated by silica gel CC using PE-EtOAc (3 : 1–1 : 9, v/v), yielding four subfractions (Fr.6.5.1-Fr.6.5.4). Compound **7** (13.2 mg) was purified from Fr.6.5.2 (96.3 mg) by preparative TLC developed with CH_2Cl_2-acetone (7 : 3, v/v).

4.4 Identification of new compounds

Magnorolin A (**1**): colorless oil; $[\alpha]_D^{20}$ −27.20 (*c* 0.05, MeOH); UV (MeOH) λ_{max} (log ε) 197 (2.21) nm; CD (MeOH) λ_{max} ($\Delta\varepsilon$) 202 (−0.62), 300 (0.03) nm; IR (KBr) ν_{max} 3398, 2926, 1776, 1709, 1439, 1163 cm^{-1}; ^1H and ^{13}C NMR data, see Tables 1 and 2; HR-ESI-MS *m/z* 305.1391 $[M - H]^+$ (calcd for $C_{17}H_{21}O_5$, 305.1394).

Magnorolin B (**2**): colorless oil; $[\alpha]_D^{20}$ −18.40 (*c* 0.05, MeOH); UV (MeOH) λ_{max} (log ε) 195 (2.30) nm; CD (MeOH) λ_{max} ($\Delta\varepsilon$) 206 (−0.06), 217 (−0.13), 228 (−0.10), 244 (−0.17) nm; IR (KBr) ν_{max} 3410, 2937, 1709, 1375, 1162, 1031 cm^{-1}; ^1H and ^{13}C NMR data, see Tables 1 and 2; HR-ESI-MS *m/z* 275.1616 $[M + Na]^+$ (calcd for $C_{15}H_{24}O_3Na$, 275.1618).

Magnorolin C (**3**): Colorless crystals; $[\alpha]_D^{20}$ −14.00 (*c* 0.05, MeOH); UV (MeOH) λ_{max} (log ε) 195 (2.87) nm; CD (MeOH) λ_{max} ($\Delta\varepsilon$) 219 (−0.38), 238 (−0.14), 253 (−0.19) nm; IR (KBr) ν_{max} 3409, 2934, 1759, 1706, 1360, 1221, 1090 cm^{-1}; ^1H and ^{13}C NMR data, see Tables 1 and 2; HR-ESI-MS *m/z* 287.1255 $[M + Na]^+$ (calcd for $C_{15}H_{20}O_4Na$, 287.1254).

Magnorolin D (**5**): colorless oil; $[\alpha]_D^{20}$ + 9.00 (*c* 0.10, MeOH); UV (MeOH) λ_{max} (log ε) 195 (2.98) nm; CD (MeOH) λ_{max} ($\Delta\varepsilon$) 197 (−3.22), 217 (−0.58), 224 (−0.74) nm; IR (KBr) ν_{max} 3419, 2927, 1774, 1710, 1638, 1261, 1105 cm^{-1}; ^1H and ^{13}C NMR data, see Tables 1 and 2; HR-ESI-MS *m/z* 331.1515 $[M + Na]^+$ (calcd for $C_{17}H_{24}O_5Na$, 331.1516).

Magnorolin E (**6**): colorless oil; $[\alpha]_D^{20}$ + 46.00 (*c* 0.10, MeOH); UV (MeOH) λ_{max} (log ε) 195 (3.06) nm; CD (MeOH) λ_{max} ($\Delta\varepsilon$) 211 (−7.01), 281 (0.30) nm; IR (KBr) ν_{max} 3420, 2934, 1777, 1628, 1142 cm^{-1}; ^1H and ^{13}C NMR data, see Tables 2 and 3; HR-ESI-MS *m/z* 331.1516 $[M + Na]^+$ (calcd for $C_{17}H_{24}O_5Na$, 331.1516).

Magnorolin F (**7**): colorless oil; $[\alpha]_D^{20}$ −10.40 (*c* 0.05, MeOH); UV (MeOH) λ_{max} (log ε) 197 (2.57) nm; CD (MeOH) λ_{max} ($\Delta\varepsilon$) 206 (−3.56), 255 (0.03) nm; IR (KBr) ν_{max} 3402, 2932, 1732, 1367, 1245, 1058 cm^{-1}; ^1H and ^{13}C NMR data, see Tables 2 and 3; HR-ESI-MS *m/z* 335.1829 $[M + Na]^+$ (calcd for $C_{17}H_{28}O_5Na$, 335.1829).

Magnorolin G (**8**): colorless oil; $[\alpha]_D^{20}$ −16.00 (*c* 0.05, MeOH); UV (MeOH) λ_{max} (log ε) 195 (2.24) nm; CD (MeOH) λ_{max} ($\Delta\varepsilon$) 201 (−0.19) nm; IR (KBr) ν_{max} 3389, 2960, 1706, 1362, 1221, 1043 cm^{-1}; ^1H and ^{13}C NMR data, see Tables 3 and 4; HR-ESI-MS *m/z* 335.1829 $[M + Na]^+$ (calcd for $C_{17}H_{28}O_5Na$, 335.1829).

Magnorolin H (**9**): colorless oil; $[\alpha]_D^{20}$ −24.40 (*c* 0.05, MeOH); UV (MeOH) λ_{max} (log ε) 195 (2.17) nm; IR (KBr) ν_{max} 3386, 2936, 1706, 1364, 1221, 1032 cm^{-1}; CD (MeOH) λ_{max} ($\Delta\varepsilon$) 200 (−0.09) nm; ^1H and ^{13}C NMR see Tables 3 and 4; HR-ESI-MS *m/z* 393.1885 $[M + Na]^+$ (calcd for $C_{19}H_{30}O_7Na$, 393.1884).

Magnorolin I (**10**): colorless oil; $[\alpha]_D^{20}$ −26.00 (*c* 0.05, MeOH); UV (MeOH) λ_{max} (log ε) 195 (2.64) nm; CD (MeOH) λ_{max} ($\Delta\varepsilon$) 211 (−0.98), 245 (0.10) nm; IR (KBr) ν_{max} 3390, 2924, 1708, 1361, 1221, 1090 cm^{-1}; ^1H and ^{13}C NMR data, see Tables 4 and 5; HR-ESI-MS *m/z* 425.2149 $[M + Na]^+$ (calcd for $C_{20}H_{34}O_8Na$, 425.2146).

Magnorolin J (**11**): colorless oil; $[\alpha]_D^{20}$ −22.40 (*c* 0.05, MeOH); UV (MeOH) λ_{max} (log ε) 195 (2.60) nm; CD (MeOH) λ_{max} ($\Delta\varepsilon$) 204 (−1.22), 235 (0.11) nm; IR (KBr) ν_{max} 3398, 2914, 1708, 1362, 1221, 1091 cm^{-1}; ^1H and ^{13}C NMR data, see Tables 4 and 5; HR-ESI-MS *m/z* 293.1722 $[M + Na]^+$ (calcd for $C_{15}H_{26}O_4Na$, 293.1723).

Magnorolin K (**12**): colorless oil; $[\alpha]_D^{20}$ −22.00 (*c* 0.05, MeOH); UV (MeOH) λ_{max} (log ε) 197 (2.52) nm; CD (MeOH) λ_{max} ($\Delta\varepsilon$) 203 (−1.13), 231 (−0.01) nm; IR (KBr) ν_{max} 3382, 2931, 1704, 1363, 1221, 1093 cm^{-1}; ^1H and ^{13}C NMR data, see Tables 4 and 5; HR-ESI-MS *m/z* 293.1721 $[M + Na]^+$ (calcd for $C_{15}H_{26}O_4Na$, 293.1723).

Magnorolin L (**15**): colorless oil; $[\alpha]_D^{20}$ + 0.80 (*c* 0.10, MeOH); UV (MeOH) λ_{max} (log ε) 224 (2.90) nm; CD (MeOH) λ_{max} ($\Delta\varepsilon$) 203 (8.18), 247 (−4.20) nm; IR (KBr) ν_{max} 3410, 2941, 1738, 1649, 1112 cm^{-1}; ^1H and ^{13}C NMR data, see Tables 4 and 5; HR-ESI-MS *m/z* 281.1396 $[M - H]^-$ (calcd for $C_{15}H_{21}O_5$, 281.1394).

X-ray crystal structure analysis of **3**: m.p. 110–112 °C; $C_{15}H_{20}O_4$, M = 287.13, orthorhombic, space group P 21 21 21, a = 7.2678(9) Å, b = 11.1560(14) Å, c = 16.214(2) Å, $\alpha = \beta = \gamma$ = 90°, V = 1314.6(3) $Å^3$, T = 100(2) K, Z = 4, crystal size 0.120 × 0.160 × 0.200 mm, μ(Cu Kα) = 0.784 mm^{-1}, 17 604 reflections measured, 2765 independent reflections (R_{int} = 0.0542). Final R indices, R_1 = 0.0336 ($I > 2\sigma(I)$), $wR(F^2)$ = 0.0899 ($I > 2\sigma(I)$), R_1 = 0.0338 (all data), $wR(F^2)$ = 0.0902 (all data). The goodness of fit on F^2 was 1.060. Flack parameter = −0.04(7). Copies of these data have been deposited in the Cambridge Crystallographic Data Centre (deposition number: CCDC 2536611).

4.5 ECD calculation

A conformational search was conducted using Spartan'14 software, and conformers with a Boltzmann distribution exceeding 1% were selected for further analysis. These conformers were then optimized using Density Functional Theory (DFT) at the B3LYP/6-311 + g (d, p) level, incorporating the PCM solvent model.[31] Subsequently, theoretical ECD calculations for the optimized conformers were using Time-Dependent Density Functional Theory (TD-DFT) at the same level of theory in MeOH with the PCM model.[31] The final ECD spectra were generated by the program SpecDis 1.7.1 program. All quantum calculations were performed using the Gaussian 16 package.

4.6 NMR calculation

Conformational searches were executed using the Spartan'14 software. The generated conformers were then optimized through DFT calculations at the B3LYP/6-311G (d, p) level in the gas phase. NMR calculations were calculated using the gauge-independent atomic orbital method at the mPW1PW91/6-

311G (d, p) level, incorporating the PCM model.[32] The resulting shielding constants for both ^{1}H and ^{13}C nuclei were directly compared with experimental chemical shifts through statistical analysis using the DP4+ probability method.[33]

4.7 Biological activities

4.7.1 Cytotoxicity assay. The K562, A549, HepG2, MDA-MB-231, and SW480 cell lines (American Type Culture Collection, Manassas, VA, USA) were cultured in either DMEM or RPMI-1640 medium supplemented with 10% fetal bovine serum (FBS) and maintained at 37 °C in a 5% CO_2 incubator. Cells were seeded into 96-well plates at a volume of 100 μL per well and allowed to adhere for 12 to 24 h. Subsequently, the cells were treated with compounds **1-16** at a concentration of 40 μM for 48 hours. After this incubation period, 20 μL of MTS solution (3-(4,5-dimethylthiazol-2-yl)-5-(3-carboxymethoxyphenyl)-2-(4-sulfophenyl)-2*H*-tetrazolium) along with 100 μL of fresh culture medium were added to each well. Following an additional 4 h incubation, the optical density (OD) was measured at 492 nm using a multifunctional microplate reader (Multiskan FC). Doxorubicin (DOX) and Taxol served as positive controls. The IC_{50} values for each compound were determined using the Reed and Muench method.[34]

4.7.2 NO inhibitory activity assay. Murine macrophage RAW 264.7 cells (Shanghai Cell Bank, Chinese Academy of Sciences) were seeded into 96-well plates containing RPMI 1640 medium (Hyclone) supplemented with 10% fetal bovine serum (FBS) and maintained in a humidified atmosphere with 5% CO_2 at 37 °C. Following a 24 h incubation period, the cells were treated with the test compounds at a maximum concentration of 50 μM, in the presence of 1 μg mL^{-1} LPS (Sigma) for 18 h. Each compound was initially dissolved in dimethyl sulfoxide (DMSO) and subsequently diluted with cell culture medium to achieve the desired concentrations. NO production was quantified by adding 100 μL of Griess reagent (comprising 1% sulfanilamide and 0.1% naphthylethylenediamine dihydrochloride in 5% phosphoric acid) to 100 μL of supernatant collected from LPS- or compound-treated cells, performed in triplicate. After a 5-minutes incubation, absorbance was measured at 570 nm using an Envision Multilabel Plate Reader (PerkinElmer Life Sciences, Inc., Boston, MA, USA). Concurrently, cell viability was assessed *via* the MTT assay to exclude potential cytotoxic effects of the test compounds. NG-Methyl-L-arginine acetate salt (L-NMMA; Sigma) served as a positive control.[35]

Author contributions

Q.-Y. Zhao: writing – original draft, formal analysis, data curation. S.-H. Yin: Investigation, data curation. X.-Y. Wang: investigation, data curation. L. Sai: investigation, data curation. L.-F. Ding: writing – review & editing, project administration. X.-D. Wu: writing – review & editing, supervision, funding acquisition.

Conflicts of interest

There are no conflicts to declare.

Data availability

CCDC 2536611 contains the supplementary crystallographic data for this paper.[36]

The datasets supporting this article are provided in the supplementary information (SI). Supplementary information: the SI includes 1D and 2D NMR spectra, HR-ESI-MS, IR, and UV data for compounds **1–3**, **5–12**, and **15**. See DOI: https://doi.org/10.1039/d6ra02737g.

Acknowledgements

This work was supported by the project of the National Natural Science Foundation of China (No. 22267022 and 82360681), Yunnan Foundamental Research Project (No. 202301AT070266), the Yunnan Fundamental Research-Joint Special Project of Kunming Medical University (No. 202401AY070001-062), Yunnan Revitalization Talent Support Program (XDYC-QNRC-2024-180), First-Class Discipline Team of Kunming Medical University (No. 2024XKTDTS12). Scientific Research Fund Project of Yunnan Provincial Education Department (No. 2025Y0366).

References

1 Editorial Committee of Flora of China, *Flora of China*, Scicence press, Beijing, 1996.
2 H. B. Wu, T. T. Liu, Z. X. Zhang, W. S. Wang, W. W. Zhu, L. F. Li, Y. R. Li and X. Chen, *Ind. Crop. Prod.*, 2018, **125**, 416–424.
3 W. D. Wu, J. L. Hu, W. Nie, M. Hu, J. D. Li, Y. F. Shen, L. F. Ding and L. D. Song, *Chem. Biodivers.*, 2022, **19**, e202200618.
4 P. V. Huyen, N. T. T. Hien, T. T. N. Hanh, N. H. H. Duyen, N. T. D. Thuan and N. H. T. Phan, *Phytochem. Rev.*, 2025, **24**, 6311–6368.
5 Y. Y. Duan, X. H. Liu, J. Q. Wu, J. M. You, F. F. Wang, X. L. Guo, T. Tang, M. Y. Liao and J. Guo, *Front. Plant Sci.*, 2022, **13**, 997868.
6 X. Zhang, F. Qian, J. J. Tan, F. J. Guo, M. Kulka, J. W. Xu and Y. M. Li, *RSC Adv.*, 2017, **54**, 34236–34243.
7 L. L. Ge, L. Chen, Q. G. Mo, G. Zhou, X. S. Meng and Y. W. Wang, *RSC Adv.*, 2018, **8**, 4362–4371.
8 M. M. Hasan, A. M. Nishan, M. H. B. Rashid, B. C. Ghos and J. Barmon, *J. Genet. Eng. Biotechnol.*, 2025, **23**, 100505.
9 Z. Q. Xie, L. F. Ding, D. S. Wang, W. Nie, J. X. Liu, J. Qin, L. D. Song, X. D. Wu and Q. S. Zhao, *Chem. Biodivers.*, 2019, **16**, e1900013.
10 S. Y. Xu, Y. Y. Tang, Y. N. Li, J. Yang, W. Gu, X. J. Hao and C. M. Yuan, *Bioorg. Chem.*, 2023, **139**, 106707.
11 D. X. Wu, J. Yang, L. H. Chen, S. Y. Xu, J. Jin, Y. N. Li, X. J. Hao and C. M. Yuan, *Phytochemistry*, 2025, **232**, 114370.

12 S. Saosathan, J. Khounvong, M. Rungrojsakul, T. Katekunlaphan, S. Tima, S. Chiampanichayakul, C. Berkland and S. Anuchapreeda, *Nat. Prod. Res.*, 2021, **35**, 988–992.
13 F. S. El-Feraly and Y. M. Chan, *J. Pharm. Sci.*, 1978, **67**, 347–350.
14 L. F. Ding, J. Su, Z. H. Pan, Z. J. Zhang, X. N. Li, L. D. Song, X. D. Wu and Q. S. Zhao, *Phytochemistry*, 2018, **155**, 182–190.
15 H. M. Cho, E. J. Park, Y. J. Park, J. Ponce-Zea, V. H. Mai, T. P. Doan, B. Ryu, Y. W. Chin and W. K. Oh, *Phytochemistry*, 2022, **200**, 113211.
16 E. Mehrotra, J. Vishwakarma, A. C. Tripathi, P. K. Sonar and S. K. Saraf, *Nat. Prod. Res.*, 2019, **33**, 568–572.
17 H. T. Binh, L. T. Linh and N. Van Ngoc, *Chem. Biodivers.*, 2025, **22**, e202403166.
18 Editorial Committee of Flora of China, *Flora of China*, Scicence press, Beijing, 1996.
19 Y. J. Lee, Y. M. Lee, C. K. Lee, J. K. Jung, S. B. Han and J. Y. Hong, *Pharmacol. Ther.*, 2011, **130**, 157–176.
20 W. Schühly, I. Khan and N. H. Fischer, *Pharm. Biol.*, 2001, **39**, 63–69.
21 L. J. Hong, G. H. Li, W. Zhou, X. B. Wang and K. Q. Zhang, *Pest. Manag. Sci.*, 2007, **63**, 301–305.
22 S. Y. Xu, F. Zhang, L. L. Tao, Y. M. Jiang, T. Huang, Y. N. Li, Z. X. Hu, J. Yang, X. J. Hao and C. M. Yuan, *Chin. J. Nat. Med.*, 2024, **22**, 265–272.
23 Q. Y. Zhao, J. D. Li, S. H. Yin, Z. Q. Li, H. L. Zhou, J. Q. Feng, W. Y. Feng, X. D. Wu and L. F. Ding, *Phytochemistry*, 2026, **244**, 114759.
24 L. F. Ding, J. X. Liu, Z. Q. Xie, D. S. Wang, W. Nie, L. D. Song, X. D. Wu and Q. S. Zhao, *Phytochem. Lett.*, 2019, **31**, 121–124.
25 H. Matsuda, T. Morikawa, K. Ninomiya and M. Yoshikawa, *Tetrahedron*, 2001, **57**, 8443–8453.
26 H. F. Wong and G. D. Brown, *Phytochemistry*, 2002, **59**, 529–536.
27 M. H. Yang, G. Blunden, A. V. Patel, M. J. O'neill and J. A. Lewis, *Planta Med.*, 1994, **60**, 390.
28 U. Jacobsson, V. Kumar and S. Saminathan, *Phytochemistry*, 1995, **39**, 839–843.
29 Y. H. He, H. Xiang, Z. J. Long, Z. X. Jin, J. F. Hu, Y. C. Mao and J. Xiong, *Bioorg. Chem.*, 2025, **158**, 108341.
30 N. U. Rehman, H. Hussain, S. A. Al-Riyami, R. Csuk, M. Khiat, G. Abbas, A. Al-Rawahi, I. R. Green, I. Ahmed and A. Al-Harrasi, *Helv. Chim. Acta*, 2016, **99**, 632–635.
31 M. Srebro-Hooper and J. Autschbach, *Annu. Rev. Phys. Chem.*, 2017, **68**, 399–420.
32 M. W. Lodewyk, M. R. Siebert and D. J. Tantillo, *Chem. Rev.*, 2012, **112**, 1839–1862.
33 N. Grimblat, M. M. Zanardi and A. M. Sarotti, *J. Org. Chem.*, 2015, **80**, 12526–12534.
34 L. Reed and H. Muench, *Am. J. Hyg.*, 1938, **27**, 493–497.
35 T. Mosmann, *J. Immunol. Methods*, 1983, **65**, 55–63.
36 CCDC 2536611: Experimental Crystal Structure Determination, 2026, DOI: 10.5517/ccdc.csd.cc2r4k5n.